Current Status of PET Technology

1

Suleman Surti and Joel S. Karp

1.1 Introduction

In recent years, PET/CT imaging has played an important clinical role as a molecular imaging tool for diagnosis and staging of cancer in patients [1]. Used predominantly with ^{18}F-fluorodeoxyglucose (FDG) as the radiotracer that acts as a glucose analog, PET/CT has significantly influenced the management of cancer patients [2, 3] and is reimbursed for initial and follow-up imaging of most cancer types [4]. In addition, PET has also been shown to play an important role in guiding cancer treatment by characterizing the tumor biology as well as monitoring tumor response to therapy [1, 5]. A more thorough overview of the current status in clinical practice is given in Chap. 2. Modern time-of-flight (TOF) PET scanners provide sufficient sensitivity and signal-to-noise ratio (SNR) performance so that clinical FDG scans with excellent diagnostic quality can be completed in 10–15 min using bed translation to cover a patient from "eyes to thighs."

Beyond FDG, there are other tracers coming into more widespread use that have very different imaging characteristics. Some of these tracers have lower photon flux because of lower dose (^{68}Ga-labelled) and/or low positron emission branching fraction (^{89}Zr-labelled or ^{124}I-labelled), requiring increased PET system sensitivity to achieve reliable quantitative images especially for dose calibration. In addition, the quantitative performance of images from some of these tracers (e.g., ^{89}Zr-labelled or ^{124}I-labelled) will also require corrections for coincidence data acquired in the presence of additional single photons. Finally, increased positron energy will require improvements in the point spread function (PSF) model used during image reconstruction to better account for the increased range of the positrons for some of these non-^{18}F-labelled tracers. Hence, while modern PET

S. Surti (✉) · J. S. Karp
University of Pennsylvania, Philadelphia, PA, USA
e-mail: surti@pennmedicine.upenn.edu; joelkarp@pennmedicine.upenn.edu

J. Zhang, M. V. Knopp (eds.), *Advances in PET*,
https://doi.org/10.1007/978-3-030-43040-5_1

scanners may provide excellent quality and quantitative FDG images, moving PET in new areas requires continued technical improvements and capabilities.

1.2 Current Status of TOF PET/CT Scanners

TOF PET scanners were originally developed in the early 1980s [6–11] when the primary application was in brain and cardiac imaging using compounds tagged with short-lived radioisotopes, such as ^{15}O-water, ^{11}C-acetate, and ^{82}Rb. While providing good timing resolution as well as reduced dead time, the primary limitations of these systems were lower sensitivity due to the use of interplane septa for 2D imaging and poor spatial resolution arising due to the choice of scintillator and photosensor. With the development of new scintillators in the late 1990s and early 2000s, a new generation of TOF PET scanners, now all PET/CT, was introduced in the mid-2000s. These scanners were optimized for the primary application of detection and staging of cancer using ^{18}F-FDG. In addition to providing good system timing resolution and spatial resolution, these scanners overcame the limitations of low sensitivity by enabling fully 3D imaging (no interplane septa). All of these scanners use lutetium-based scintillators (LSO and LYSO) and utilize light-sharing detectors to achieve high spatial resolution (4–5 mm) with photomultiplier tubes (PMTs) of 25–39 mm size. Due to the detector design, the coincidence timing resolution of these scanners lies within the range of 450–600 ps – very similar to the scanners developed in the 1980s but with superior spatial resolution and sensitivity. Recent years have seen an introduction of a new solid-state-based photosensor (silicon photomultiplier, or SiPM) that provides excellent intrinsic timing performance on par or better than the conventional PMTs while providing flexibility in detector size that is not available with PMTs. This has led to the commercial development of a new generation of "digital" PET scanners using SiPM arrays with reduced or almost no light sharing in the detector design. These new scanners have much improved system coincidence timing resolution (210–390 ps) with similar or improved spatial resolution through the use of smaller crystals. The benefits of TOF for clinical imaging were well established [12–18], and so it is expected that improved TOF resolution will increase these benefits, particularly for patients with larger body mass index (BMI).

1.3 Hardware Design

1.3.1 Scintillator

As mentioned earlier, lutetium-based scintillators are currently being used in all modern commercial whole-body TOF PET scanners. This choice is driven by the combination of high stopping power, high light output, and fast decay time of these scintillators which leads to high system sensitivity as well as very good energy and spatial and timing resolutions – all necessary characteristics for a modern fully 3D

TOF PET system [19–21]. The two scintillators used most commonly are closely related: cerium-doped lutetium oxy-orthosilicate (Lu_2SiO_5(Ce) or LSO(Ce)) and lutetium-yttrium oxy-orthosilicate ($Lu_{1.8}Y_{0.2}SiO_5$(Ce) or LYSO(Ce)). In the early to mid-1990s, LSO(Ce), usually referred to as LSO, was first developed and introduced as a PET scintillator [22] as a replacement for BGO. At the time BGO was the primary scintillator being used in commercial PET but had limitations due to its poor light output and long decay time – less than ideal properties for fully 3D PET in comparison with NaI(Tl), which was also in use commercially [19]. While LSO was first used in a small animal PET scanner [23] and subsequently incorporated into a brain [24, 25] and a whole-body PET scanner [26], it was later recognized that it also had very good timing resolution that could be used in the development of TOF PET scanners [20, 21]. Following a similar trajectory, LYSO was first utilized in a dedicated small animal PET scanner [27] and subsequently used in the production of a new generation of commercial TOF PET/CT system [28]. While the current version of the Lu-based scintillators all uses varying levels of Ce doping, there have been efforts to change the dopant in order to achieve improved performance. For instance, a co-doped version of LSO using calcium has been developed with increased light output and shorter decay time than the LSO(Ce) scintillator [29], leading to further improvements in timing resolution [30]. Similarly, calcium and magnesium co-doped versions of LYSO have also been reported to produce higher light output than cerium-doped LYSO [31], implying improved timing performance. Thus, there is potential for improved lutetium-based scintillators that could be a direct replacement for the current versions of commercially used LSO and LYSO.

While BGO is relatively inexpensive and was a preferred PET scintillator prior to the development of LSO, the slow time scale of the luminescence process made it impossible to use it for TOF PET. However, it has been noted that the passage of charged electrons produced within BGO by the annihilation photons leads to the emission of Cherenkov light that can be detected by the SiPM devices (high quantum efficiency) [32]. The time scale of Cherenkov emission is very fast leading to a very fast signal and potential for fast timing resolution that is appropriate for TOF PET [33]. Several studies have been performed recently [34, 35] with best results indicating a coincidence timing resolution as good as 330 ps (FWHM) can be achieved with a 20-mm-long crystal [34]. However, the light output from Cherenkov emission is very low; thus, it is still necessary to utilize the (slower) scintillation light to determine both energy and spatial localization of the gamma interaction, and it remains to be seen how practical it is to use Cherenkov timing for TOF PET imaging with BGO.

1.3.2 Photosensor

Since the development of early PET scanners, PMTs have been the photosensor of choice for all clinical systems. The high gain and consequently high signal-to-noise ratio of the PMT signal lead to very good energy resolution, and plano-concave photocathodes combined with careful dynode design have made it possible to

achieve very fast timing with cost-effective PMTs in sizes suitable (25–39 mm diameter) to combine with multi-crystal PET detector arrays. The development of new super and ultra bialkali, plano-concave photocathodes with increased quantum efficiency (QE) and improved dynode structure to improve signal rise time has led to further improvements in the timing resolution achieved with PMTs. Single-channel PMTs have been the standard in PET systems where a light-sharing method is used to achieve spatial resolution significantly better than the PMT size. In addition to new photocathode materials, new fabrication methods have led to the development of fast multi-anode PMTs where a single photocathode is shared by several small anodes in a single PMT package. A fairly common multi-anode PMT design has a 5 × 5 cm^2 cross section with an 8 × 8 or 16 × 16 array of anodes for readout (Fig. 1.1). These PMTs provide additional flexibility in developing fast PET detectors with minimal light sharing to achieve high detector spatial resolution; however, their complex design makes them considerably more expensive than the single-channel PMT.

The last 15–20 years has seen the introduction of a new solid-state photosensor (SiPM) that is compact and fast, has high gain and low noise, and is insensitive to magnetic fields [36–40]. Although this technology was initially expensive, the cost has decreased as the devices become more widely used. Details about SiPM technology are discussed later in Chaps. 3–6.

Since SiPM devices can be fabricated in small sizes, as opposed to PMTs, they provide great flexibility in developing high-resolution PET detectors. They also operate at low bias voltage (few tens of volts) as opposed to PMTs (about thousand volts), and being solid-state technology can be made nonmagnetic that is necessary for PET/MR scanners that incorporate a PET detector ring inside the magnet bore

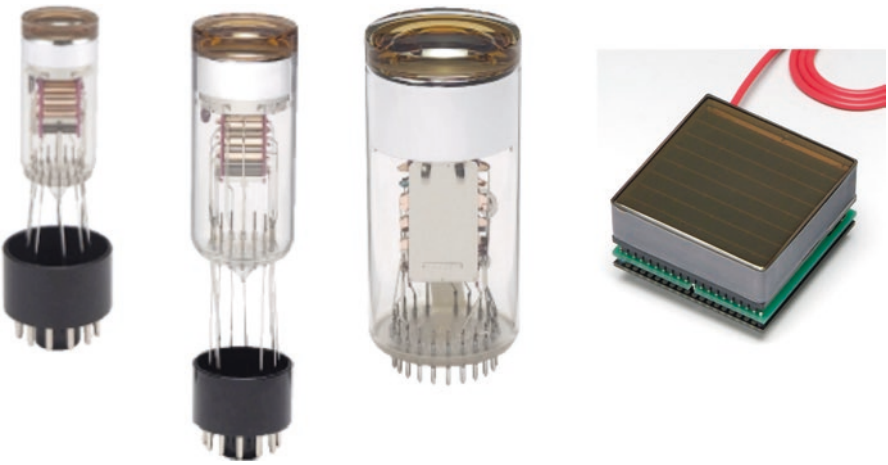

Fig. 1.1 From left to right, pictures of 25 mm diameter (R9800), 38 mm diameter (R9420), and 51 mm diameter (R7724) single-channel PMTs and a 64-channel H8500 MAPMT. All PMTs are manufactured by Hamamatsu. The H8500 is 5 × 5 cm^2 in size and the individual anodes are about 6.25 × 6.35 mm^2. (Images courtesy of Hamamatsu)

to enable simultaneous PET and MR scanning. Additional work to further improve the performance of SiPMs is ongoing, ranging from increase in photon detection efficiency (PDE) due to increased microcell density and quantum efficiency, as well as the development of 3D digital SiPMs (wafer-level integration of the SiPM and readout electronics). While the current version of digital SiPM technology [41, 42] has increased the flexibility and performance to some degree, there are some limitations in this design. For instance, a single time-to-digital converter (TDC) is used to obtain timing information for one or more SiPM channels. However, there is a timing skew attached to the signal from each microcell based on its location within the SiPM channel that leads to a degradation of the timing performance of the SiPM channel due to the use of a common TDC. One aspect of 3D digital SiPM development work is to fabricate a dedicated TDC for each microcell within a SiPM channel that will likely lead to a device with significantly improved intrinsic timing performance. Early SiPM devices were a few millimeters in size, but recent fabrication techniques have led to the development of larger arrays of these devices that are suitable for use in modern PET scanners by coupling to comparably sized scintillator arrays. Early SiPM arrays were fabricated using discrete SiPM devices connected via bond wires on a common printed circuit board that led to relatively large dead areas between each SiPM channel and hence a lower device PDE. More recent developments have led to the production of SiPM arrays using through-silicon vias (TSV) technology to interconnect the individual SiPM channels and significantly reduce the dead area due to classical wire bonding. An ideal solution will be to fabricate the entire SiPM array on common wafer to produce what are called monolithic arrays. However, a disadvantage of this method is that fabrication errors could lead to large variations in performance of individual channels on the device leading to suboptimal performance – a limitation that is not present in the discrete arrays where each channel can be chosen to provide a uniform performance.

1.3.3 Detector Design

The properties of the chosen scintillator and photosensor define the best intrinsic performance that can be achieved by the PET detector. In particular, the crystal size determines the detector spatial resolution (cross section) and sensitivity (thickness) as well as light output that in turn affects the detector energy and timing resolution. Standard commercial PET detectors have used Lu-based crystals that are 4–5 mm wide and 18–25 mm thick. Until the recent advent of SiPM, PET detectors were comprised of rectangular crystal arrays coupled to large PMTs (25–39 mm in diameter) via a light-sharing technique such as that utilized in block detectors [43], quadrant sharing block detectors [44], or the pixelated Anger-logic detectors [45] (see examples in Fig. 1.2). These types of detector designs are still in use in modern PET/CT systems from all major manufacturers [46–49]. While all of these systems provide very good overall performance, their TOF performance (coincidence timing resolution in the range of 400–550 ps) is limited due to the practical choices made in the detector design: light loss and transit time dispersion of scintillation photons

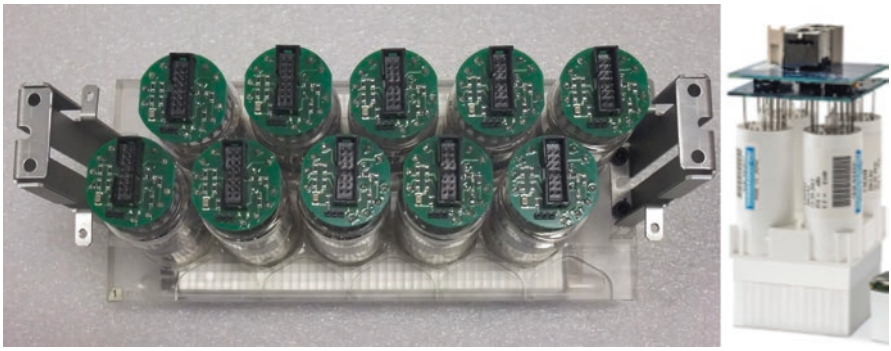

Fig. 1.2 Picture of a single detector module from a Philips Gemini TF scanner using a pixelated Anger-logic detector design (left) and a Siemens Biograph mCT scanner using a block detector. The Gemini TF (and newer Ingenuity TF) detector consists of a 23 × 44 array of 4 × 4 × 22 mm^3 LYSO crystals coupled to a hexagonal array of 39-mm-diameter single-channel PMTs. The open crystal area visible along the lower edge of the detector module would be read out with another row of PMTs that are not shown here which will straddle this and the neighboring module to form a continuous detector ring in the scanner. The mCT detector consists of a 13 × 13 array of 4 × 4 × 20 mm^3 LSO crystals coupled to a 2 × 2 square array of 25-mm-diameter single-channel PMTs. Compared to the Gemini TF detector, each mCT detector is completely independent of neighboring detector modules. (Pictures courtesy of Philips Healthcare and Siemens Healthineers)

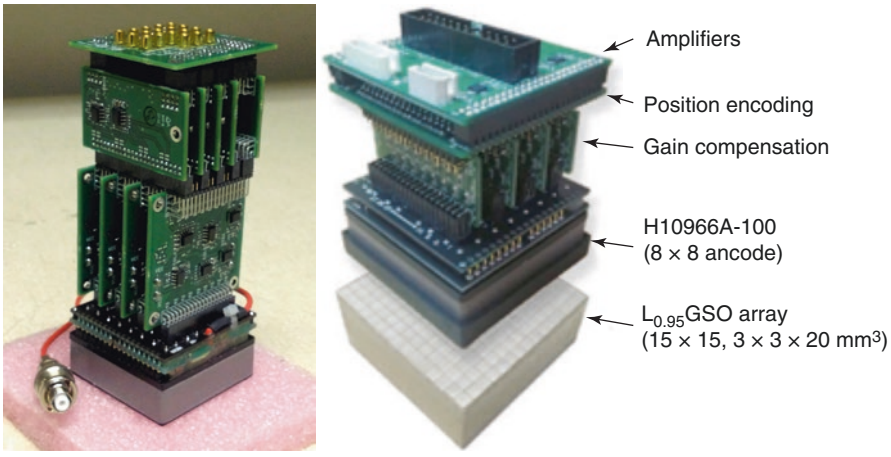

Fig. 1.3 Pictures of two multi-anode PMT-based PET detectors used in a dedicated breast imaging PET/tomosynthesis system under development at the University of Pennsylvania and a research whole-body PET scanner. The detector on the left uses a 32 × 32 array of 1.5 × 1.5 × 15 mm^3 LYSO crystals, while the one on the right uses a 15 × 15 array of 3 × 3 × 20 mm^3 LGSO crystals. (The figures are reprinted with permission from [51] (left) and [52] (right))

as they undergo multiple reflections within a long, narrow crystal [20] and the degrading effects due to the light-sharing mechanism of these PMT-based detectors [50]. Some of these limitations can be mitigated with the use of multi-anode PMTs (MAPMT) that require minimal or no light sharing due to small size of the individual anodes (Fig. 1.3) [51]. As shown in Fig. 1.3, one can also appreciate the

significant overhead of associated electronics per detector, although a commercial implementation would reduce the size of this prototype design. Nevertheless, a complete prototype TOF PET system has been recently developed with these electronics incorporated and with coincidence timing resolution of 340 ps [52]. A bigger drawback of MAPMT-based detectors is that the cost of the MAPMTs is significantly high compared to single-channel PMTs. The advent of SiPM arrays with cost approaching that of single-channel PMTs per unit detector area has therefore made the use of MAPMTs in TOF PET scanners less likely since they are not cost-effective with the existing technology. Compared to the multi-anode PMTs, SiPM arrays also present a more flexible and practical alternative to achieving excellent detector performance. For SiPM arrays, all the electronics as shown in Fig. 1.3 can be replaced by developing a dedicated ASIC where all the electronics are placed on a chip. While this can be a very costly development, it is easy to make copies for use with multiple detectors. Alternately, for the digital SiPM array from Philips (Philips Digital Photon Counter, or PDPC), most of the event processing is done in a field-programmable gate arrays (FPGA). While the ideal detector design will match each SiPM channel to a single crystal (Fig. 1.4), commercial detectors using some light sharing have already shown excellent overall performance. Commercial, digital PET/CT using SiPM devices is already available from the major manufacturer providing coincidence timing resolution of the PET system in the range of 210–390 ps.

In the future, new detectors with improved scintillators or photosensors promise additional improvements. For instance, 22-mm-thick LYSO scintillators 1-1 coupled to a new generation of SiPMs with improved PDE have shown benchtop measurements of <150 ps coincidence timing resolution [53]. A commercial PET scanner comprises tens of thousands of individual crystals, and a similar number of

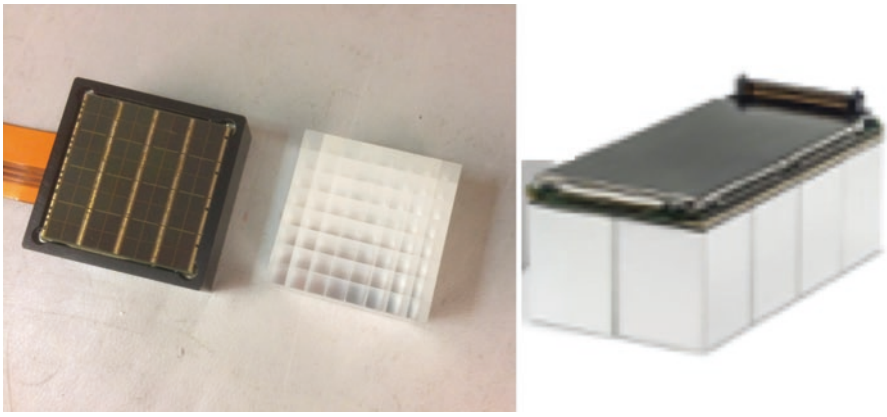

Fig. 1.4 (Left) Picture of PDPC digital SiPM array (8 × 8 array, 3.6 cm × 3.6 cm) placed next to an 8 × 8 array of LYSO crystals. The LYSO crystal cross section is matched to individual channels of the PDPC array, and 360 of such detector arrays are used in the complete Philips Vereos PET/CT scanner. (Right) A 4 × 2 array (6.4 cm × 3.2 cm) of mini-blocks configured as a detector in the Siemens Biograph Vision PET/CT scanner (a total of 304 detectors are present in the scanner). Each mini-block consists of a 4 × 4 channel (1.6 cm × 1.6 cm) SiPM array coupled to a 5 × 5 array of LSO crystals. A dedicated ASIC array is coupled to the top (back of SiPM array) in the Siemens detector. (Pictures courtesy of Philips Healthcare and Siemens Healthineers)

electronic channels (including TDCs) will be needed in a 1-1 coupled detector design. Even if some signal multiplexing is utilized, the number of electronic channels is still very large, requiring careful calibrations in order to maintain the benchtop performance. An intriguing option is the use of a single monolithic scintillation detector instead of an array of long, narrow crystals coupled to a SiPM array. These detectors reduce or remove the degrading effect of multiple reflections of scintillation photons within a long, narrow crystal while also simplifying the need for assembling large crystal arrays and show great promise in achieving both good spatial resolution with depth-of-interaction (DOI) measurement and timing resolution [54, 55]. Recent work has shown that spatial resolution of <1.5 mm (FWHM) and coincidence timing resolution of <150 ps can be achieved in such a detector design with crystals similar in thickness to those used commercially (~2 cm) [56]. While the spatial resolution at the FWHM level is the best reported value for detectors of this thickness, the spatial response is non-Gaussian with long tails suggesting that imaging performance will be somewhat compromised relative to a detector achieving similar FWHM with a Gaussian response function. A potential drawback is the need for significant detector calibrations and the complexity of position and timing estimation algorithm. Despite these limitations, these measurements demonstrate potential for further improvement in performance of full systems. It is notable that a PET scanner based on 8-mm-thick monolithic detectors is commercially available for small animal imaging [50]. This system provides very high spatial resolution with DOI correction that allows a PET scanner with a small diameter detector ring to achieve uniform spatial resolution of ~ 1 mm throughout the imaging field of view.

1.4 Software Algorithms

In the last two decades, significant progress has been made in the implementation of statistical ordered subset expectation maximization (OS-EM) algorithms for routine use in clinical PET. Compared to analytical algorithms, these provide better noise characteristics in the image, which is especially relevant for the lower sensitivity of clinical PET scanners. The advent of new TOF PET scanners in the mid- to late 2000s led to an extension of these algorithms to TOF-assisted OS-EM algorithms where each collected event along an LOR is back-projected over a limited LOR length (determined by the TOF difference of the coincident photons and the system timing resolution) instead of its entire extent within the patient or imaging object leading to reduced noise propagation during image reconstruction [57, 58]. Regularization techniques can lead to a further reduction in reconstructed image noise [59] and have been implemented commercially. While noise reduction is an important component of optimizing image quality, it is also important to maintain quantitative accuracy with these techniques. Spatial resolution modeling (also referred to as PSF modeling) within the reconstruction algorithm can also improve image quality since it corrects for degrading effects, such as detector resolution, positron range, and parallax error, and effectively leads to improved spatial

resolution in the reconstructed images [60, 61]. Finally, joint estimation of emission and attenuation images has been investigated for many years [62], with an eye toward avoiding the use of the CT images for attenuation correction. For non-TOF PET data, this approach does not provide robust results, since the cross talk between the two reconstructions makes it impossible to uniquely determine both attenuation and emission distributions independently. With TOF information, simultaneous attenuation-emission reconstruction approaches have been revisited [63] with great promise [62, 64, 65]. Although there is still a need for a relative scaling of the emission and transmission reconstructions, the cross talk between them is significantly reduced by incorporating the TOF information into the joint estimation. While it is unlikely that PET will be used routinely without CT for clinical purposes, there are situations that would benefit from being able to provide quantitative images without the radiation dose from the CT, such as pediatric imaging.

1.5 Conclusion

The last 20 years has seen significant improvements in PET instrumentation leading to greatly enhanced imaging performance. These improvements have been driven by technological hardware advancements beginning with improved scintillator characteristics and new photosensors leading to new digital detector designs using primarily SiPMs. A consequence of these advancements has been an improvement in intrinsic system sensitivity while acquiring data exclusively in fully 3D mode and a commercial implementation of TOF imaging with both PET/CT and PET/MR systems. In parallel, software developments utilizing the advantages of improved or expanded information present in PET data have led to image reconstruction methods that lead to greatly improved signal-to-noise ratio in the images. Consequently, routine clinical exams can be performed in <10 min while also opening new avenues for PET imaging utilizing either new radiotracers or using new imaging protocols.

References

1. Kircher MF, Hricak H, Larson SM. Molecular imaging for personalized cancer care. Mol Oncol. 2012;6(2):182–95.
2. Von Schulthess GK, Steinert HC, Hany TF. Integrated PET/CT: current applications and future directions. Radiology. 2006;238(2):405–22.
3. Juweid ME, Cheson BD. Positron-emission tomography and assessment of cancer therapy. N Engl J Med. 2006;354(5):496–507.
4. Buck AK, et al. Economic evaluation of PET and PET/CT in oncology: evidence and methodologic approaches. J Nucl Med. 2010;51(3):401–12.
5. Mankoff DA, et al. Development of companion diagnostics. Semin Nucl Med. 2016;46(1):47–56.
6. Ter-Pogossian MM, et al. PETT VI: a positron emission tomograph utilizing cesium fluoride scintillation detectors. J Comput Assist Tomogr. 1982;6:125–33.
7. Ter-Pogossian M, et al. Super PETT I: a positron emission tomograph utilizing photon time-of-flight information. IEEE Trans Med Imaging. 1982;M1-1(3):179–87.

8. Gariod R, et al. The "LETI" positron tomograph architecture and time-of-flight improvements. In: Proceedings of IEEE workshop on time-of-flight emission tomography. St. Louis: Washington University; 1982.
9. Wong WH, et al. Performance characteristics of the University of Texas TOF PET-I Camera. J Nucl Med. 1984;25(5):46–7.
10. Lewellen TK, et al. Performance measurements of the SP3000/UW time-of-flight positron emission tomograph. IEEE Trans Nucl Sci. 1988;35(1):665–9.
11. Mazoyer B, et al. Physical characteristics of TTV03, a new high spatial resolution time-of-flight positron tomograph. IEEE Trans Nucl Sci. 1990;37(2):778–82.
12. Daube-Witherspoon ME, et al. Determination of accuracy and precision of lesion uptake measurements in human subjects with time-of-flight PET. J Nucl Med. 2014;55:602–7.
13. Karp JS, et al. Benefit of time-of-flight in PET: experimental and clinical results. J Nucl Med. 2008;49(3):462–70.
14. Surti S, et al. Impact of TOF PET on whole-body oncologic studies: a human observer detection and localization study. J Nucl Med. 2011;52:712–9.
15. Conti M. Why is TOF PET reconstruction a more robust method in the presence of inconsistent data? Phys Med Biol. 2011;56:155–68.
16. Kadrmas DJ, et al. Impact of time-of-flight on PET tumor detection. J Nucl Med. 2009;50(8):1315–23.
17. Kadrmas DJ, et al. Effect of scan time on oncologic lesion detection in whole-body PET. IEEE Trans Nucl Sci. 2012;59:1940–7.
18. Lois C, et al. An assessment of the impact of incorporating time-of-flight information into clinical PET/CT imaging. J Nucl Med. 2010;51:237–45.
19. Muehllehner G, Karp JS, Surti S. Design considerations for PET scanners. Q J Nucl Med. 2002;46(1):16–23.
20. Moses WW, Derenzo SE. Prospects for time-of-flight PET using LSO scintillator. IEEE Trans Nucl Sci. 1999;46(3):474–8.
21. Moses WW. Time of flight in PET revisited. IEEE Trans Nucl Sci. 2003;50(5):1325–30.
22. Melcher CL, Schweitzer JS. Cerium-doped lutetium oxyorthosilicate - a fast, efficient new scintillator. IEEE Trans Nucl Sci. 1992;39(4):502–5.
23. Cherry SR, et al. MicroPET: a high resolution PET scanner for imaging small animals. IEEE Trans Nucl Sci. 1997;44:1161–6.
24. Schmand M, et al. Performance results of a new DOI detector block for a high resolution PET-LSO research tomograph HRRT. IEEE Trans Nucl Sci. 1998;45(6):3000–6.
25. Wienhard K, et al. The ECAT HRRT: performance and first clinical application of the new high resolution research tomograph. IEEE Trans Nucl Sci. 2002;49(1):104–10.
26. Spinks TJ, Bloomfield PM. A comparison of count rate performance for 15-O-water blood flow studies in the CTI HR+ and Accel tomographs in 3D mode. In: IEEE nuclear science symposium and medical imaging conference. Norfolk; 2002.
27. Surti S, et al. Imaging performance of A-PET: a small animal PET camera. IEEE Trans Med Imaging. 2005;24(7):844–52.
28. Surti S, et al. Performance of Philips Gemini TF PET/CT scanner with special consideration for its time-of-flight imaging capabilities. J Nucl Med. 2007;48(3):471–80.
29. Spurrier MA, et al. Effects of Ca2+ Co-doping on the scintillation properties of LSO:Ce. IEEE Trans Nucl Sci. 2008;55(3):1178–82.
30. Szczesniak T, et al. Timing resolution and decay time of LSO crystals Co-doped with calcium. IEEE Trans Nucl Sci. 2010;57(3):1329–34.
31. Blahuta S, et al. Evidence and consequences of Ce in LYSO: Ce, Ca and LYSO: Ce, Mg single crystals for medical imaging applications. IEEE Trans Nucl Sci. 2013;60(4):3134–41.
32. Brunner SE. Fast single photon detection for scintillation and cherenkov applications using silicon photomultipliers. 2014, TU Vienna.
33. Brunner SE, et al. Studies on the Cherenkov effect for improved time resolution of TOF-PET. IEEE Trans Nucl Sci. 2014;61:443–7.

34. Brunner SE, Schaart DR. BGO as a hybrid scintillator / Cherenkov radiator for cost-effective time-of-flight PET. Phys Med Biol. 2017;62(11):4421–39.
35. Kwon SI, et al. Bismuth germanate coupled to near ultraviolet silicon photomultipliers for time-of-flight PET. Phys Med Biol. 2016;61:L38.
36. Buzhan P, et al. An advanced study of silicon photomultiplier. ICFA Instrum Bullet. 2001;23:28.
37. Buzhan P, et al. Silicon photomultiplier and its possible applications. Nucl Inst Methods Phys Res A. 2003;504(1–3):48–52.
38. Bisello D, et al. Metal-Resistive layer-Silicon (MRS) avalanche detectors with negative feedback. Nucl Inst Methods Phys Res A. 1995;360(1–2):83–6.
39. Golovin V, Saveliev V. Novel type of avalanche photodetector with Geiger mode operation. Nucl Inst Methods Phys Res A. 2004;518(1–2):560–4.
40. Renker D. Geiger-mode avalanche photodiodes, history, properties and problems. Nucl Inst Methods Phys Res A. 2006;567(1):48–56.
41. Frach T, et al. The digital silicon photomultiplier: principle of operation and intrinsic detector performance. In: IEEE nuclear science symposium and medical imaging conference. Orlando; 2009.
42. Degenhardt C, et al. The digital silicon photomultiplier ; a novel sensor for the detection of scintillation light. In: IEEE nuclear science symposium and medical imaging conference. Orlando; 2009.
43. Casey ME, Nutt R. A multicrystal two dimensional BGO detector system for positron emission tomography. IEEE Trans Nucl Sci. 1986;33(1):460–3.
44. Wong WH, et al. A 2-dimensional detector decoding study on BGO arrays with quadrant sharing photomultipliers. IEEE Trans Nucl Sci. 1994;41(4):1453–7.
45. Surti S, et al. Optimizing the performance of a PET detector using discrete GSO crystals on a continuous lightguide. IEEE Trans Nucl Sci. 2000;47:1030–6.
46. Jakoby BW, et al. Physical and clinical performance of the mCT time-of-flight PET/CT scanner. Phys Med Biol. 2011;56(8):2375–89.
47. Bettinardi V, et al. Physical performance of the new hybrid PET/CT Discovery-690. Med Phys. 2011;38(10):5394–411.
48. Kolthammer JA, et al. Performance evaluation of the ingenuity TF PET/CT scanner with a focus on high count-rate conditions. Phys Med Biol. 2014;59(14):3843–59.
49. Burr KC, et al. A new modular and scalable detector for a time-of-flight PET scanner. In: IEEE nuclear science symposium and medical imaging conference. Anaheim; 2012.
50. Moses WW, Ullisch M. Factors influencing timing resolution in a commercial LSO PET camera. IEEE Trans Nucl Sci. 2006;53(1):78–85.
51. Krishnamoorthy S, et al. Design and performance of a high spatial-resolution, time-of-flight PET detector. IEEE Trans Nucl Sci. 2014;61:1092–8.
52. Son J-W, Ko GB, Won JY, Yoon HS, Lee JS. Development and performance evaluation of a time-of-flight positron emission tomography detector based on a high-quantum-efficiency multi-anode photomultiplier tube. IEEE Trans Nucl Sci. 2014;63:44–51.
53. Ferri A, et al. 100ps coincidence time resolution with LYSO coupled to NUV-HD SiPMs. In: IEEE nuclear science symposium and medical imaging conference. San Diego; 2015.
54. van Dam HT, et al. Sub-200 ps CRT in monolithic scintillator PET detectors using digital SiPM arrays and maximum likelihood interaction time estimation. Phys Med Biol. 2013;58(10):3243–58.
55. Seifert S, et al. First characterization of a digital SiPM based time-of-flight PET detector with 1 mm spatial resolution. Phys Med Biol. 2013;58(9):3061–74.
56. Borghi G, et al. A 32 mm × 32 mm × 22 mm monolithic LYSO:Ce detector with dual-sided digital photon counter readout for ultrahigh-performance TOF-PET and TOF-PET/MRI. Phys Med Biol. 2016;61(13):4929–49.
57. Popescu LM. Iterative image reconstruction using geometrically ordered subsets with list-mode data. In: IEEE nuclear science symposium and medical imaging conference. Rome; 2004.
58. Daube-Witherspoon ME, et al. Comparison of list-mode and DIRECT approaches for time-of-flight PET reconstruction. IEEE Trans Med Imaging. 2012;31:1461–71.

59. Asma E, et al. Accurate and consistent lesion quantitation with clinically acceptable penalized likelihood images. In: 2012 IEEE nuclear science symposium and medical imaging conference. Anaheim; 2012.
60. Panin VY, et al. Fully 3-D PET reconstruction with system matrix derived from point source measurements. IEEE Trans Med Imaging. 2006;25(7):907–21.
61. Tong S, Alessio AM, Kinahan PE. Noise and signal properties in PSF-based fully 3D PET image reconstruction: an experimental evaluation. Phys Med Biol. 2010;55(5):1453–73.
62. Panin VY, Aykac M, Casey ME. Simultaneous reconstruction of emission activity and attenuation coefficient distribution from TOF data, acquired with external transmission source. Phys Med Biol. 2013;58:3649–69.
63. Defrise M, Rezaei A, Nuyts J. Time-of-flight PET data determine the attenuation sinogram up to a constant. Phys Med Biol. 2012;57:885–99.
64. Rezaei A, et al. Simultaneous reconstruction of activity and attenuation in time-of-flight PET. IEEE Trans Med Imaging. 2012;31:2224–33.
65. Nuyts J, Rezaei A, Defrise M. ML-reconstruction for TOF-PET with simultaneous estimation of the attenuation factors. In: 2012 IEEE nuclear science symposium and medical imaging conference. Anaheim: IEEE; 2012.